Mixing and phase separation at supercritical and transcritical pressures

Stefan Hickel

Faculty of Aerospace Engineering
Technische Universiteit Delft (TU Delft)
Kluyverweg 1, 2629 HS Delft, The Netherlands.
S.Hickel@tudelft.nl

Jan Matheis

Department of Mechanical Engineering
Technische Universität München (TUM)
Boltzmannstr. 15, 85748 Garching, Germany.
Jan.Matheis@tum.de

ABSTRACT

We have developed a thermodynamically consistent and tuning-parameter-free two-phase model for Eulerian large-eddy simulations (LES) of liquid-fuel injection and mixing at high pressure. The model is based on cubic equations of state and vapor-liquid equilibrium calculations. It can represent the coexistence of supercritical states and multi-component subcritical two-phase states via a homogeneous mixture approach without any semi-empirical break-up and evaporation models. Computational results for liquid-fuel injection at transcritical operating conditions are found to agree very well with available experimental data for the ECN Spray A.

INTRODUCTION

We discuss the large-eddy simulation (LES) of high-pressure liquid-fuel injection, with an emphasis on the physical modeling of the turbulent mixing of supercritical and transcritical fluids. The considered setup is based on the Spray A benchmark case of the Engine Combustion Network (ECN) and consists of a cold dodecane jet ($CH_3(CH_2)_{10}CH_3$ at 363 K) that is injected with about 600 m/s into a warm nitrogen (N_2) atmosphere at 900 K and a pressure of 60 bar. This high pressure exceeds the critical pressure p_c of both components and results in a compressed liquid ($p > p_c$, $T < T_c$) and a gas-like ($T > T_c$, $p > p_c$) state of the two pure species. However, the critical pressure of certain mixtures of the two species is much higher than the critical pressure of the pure species and also higher than the Spray A operating pressure, such that the mixture locally enters a two-phase region and interfaces between liquid and gas phases may appear during the mixing process. We refer to such conditions as transcritical operating conditions.

Recent experimental data and theoretical studies of the ECN Spray A have received considerable attention in the community, see Dahms *et al.* (2013) and Dahms & Oefelein (2013), e.g., and questioned the established paradigm of classic spray atomization (primary and secondary breakup, evaporation of droplets) for high-pressure and high-temperature fuel injection. Above certain pressures and temperatures a *dense fluid mixing* with diminishing surface tension was observed in the near-field of n-dodecane sprays, see, e.g., Manin *et al.* (2014). With improved optical diagnostics, Crua *et al.* (2015) pushed recently the boundaries above which this transition takes place towards higher pressures and temperatures. Hence, the nominal operating conditions of Spray A now seem to be more within the subcritical regime. Moreover, their measurements showed that the fluid does not reach the *dense-fluid mixing* state instantaneously and classical evaporation does occur for some time. Therefore, classical two-phase phenomena appear to be relevant for high-pressure and high-temperature fuel injection and must be taken into account by the physical models employed for simulations.

Previous numerical simulations of ECN Spray A have either modeled the spray with Lagrangian particle tracking (LPT) methods, that is, as a classical two-phase spray with sharp gas-liquid interfaces evolving according to models for first- and secondary breakup and evaporation, or with a single-phase dense-gas approach, arguing that the high pressure and temperature lead to a diffusion-like mixing process with negligible surface tension. Both approaches can be justified but have obvious limitations when applied to transcritical operating conditions that correspond to a transition regime between classical spray dynamics and miscible mixing. Standard LPT methods are very efficient computationally and yield impressive results for dilute two-phase flows, but the models are sensitive to empirical calibration parameters and usually neglect real-gas effects and dissolved ambient gases in the liquid fuel phase, which can become substantial at high pressures (Balaji *et al.*, 2011; Qiu & Reitz, 2015). The single-phase dense-gas approach, on the other hand, does not include the effect of phase separation and may thus lead to unphysical or ill defined states if part of the flow is subcritical.

To improve on these limitations, we have recently developed a thermodynamically consistent detailed multi-species two-phase model for the Eulerian LES of turbulent mixing under high pressures (Matheis & Hickel, 2016, 2017). The thermodynamics model is based on cubic EOS and vapor-liquid equilibrium (VLE) calculations. It can represent multi-component supercritical states as well as coexisting multi-component subcritical two-phase states in a computational cell without empirical tuning parameters.

PHYSICAL MODEL

We solve the three-dimensional compressible multicomponent Navier-Stokes equations in a fully conservative finite-volume formulation for mass density ρ, linear-momentum density $\rho\mathbf{u}$, total-energy density $E = \rho e + \frac{1}{2}\rho\mathbf{u}\cdot\mathbf{u}$ and partial mass densities ρY_i of species $i = \{1\dots N_c\}$:

$$\partial_t \rho + \nabla\cdot(\rho\mathbf{u}) = 0 \tag{1}$$

$$\partial_t \rho Y_i + \nabla\cdot(\rho Y_i\mathbf{u}) = \nabla\cdot\mathbf{J}_i \tag{2}$$

$$\partial_t \rho\mathbf{u} + \nabla\cdot(\rho\mathbf{uu} + \mathbf{I}p) = \nabla\cdot\tau \tag{3}$$

$$\partial_t E + \nabla\cdot[(E + p)\mathbf{u}] = \nabla\cdot(\mathbf{u}\cdot\tau - \mathbf{q}) \ . \tag{4}$$

The viscous stress tensor is modeled according to the Stokes hypothesis for a Newtonian fluid as

$$\tau = \mu\nabla\mathbf{u} + (\nabla\mathbf{u})^T - \frac{2}{3}\mu\,\mathbf{I}\,\nabla\cdot\mathbf{u}, \tag{5}$$

with μ being the dynamic viscosity and $\mathbf{I}$ the unit tensor. We model viscosity and thermal conductivity with correlations given by Chung *et al.* (1988). The diffusional fluxes are calculated via Fick's law

$$\mathbf{J}_i = \rho D_i\nabla Y_i - Y_i\sum_{j=1}^N \rho D_j\nabla Y_j \ , \tag{6}$$

where

$$D_i = \frac{1 - z_i}{\sum_{j \neq i}^{N} z_j D_{ij}^{-1}} \tag{7}$$

is an effective binary diffusion coefficient for the diffusion of species i into the rest of the mixture and z_i denotes the mole fraction of species i. The physical binary mass diffusion coefficients D_{ij} are modeled according to Chapman and Enskog theory (see e.g. Prausnitz $et\ al.$, 1998). The vector

$$\mathbf{q} = -\kappa \nabla T - \sum_{i=1}^{N} h_i \mathbf{J}_i \tag{8}$$

consists of heat conduction the enthalpy flux by species diffusion, where κ is the thermal conductivity, T is the temperature, and h_i is the partial enthalpy of species i.

The thermodynamics model is based on the cubic Peng & Robinson (1976) equation of state (PR-EOS),

$$p(\underline{v}, T, \mathbf{z}) = \frac{\mathcal{R}T}{\underline{v} - b} - \frac{a\alpha}{\underline{v}^2 + 2b\underline{v} - b^2}, \tag{9}$$

where the pressure p is a function of the molar volume $\underline{v}$, temperature T and the molar composition $\mathbf{z} = \{z_1 \ldots z_{N_c}\}$. Here and in the following, all intensive thermodynamic properties are expressed as molar quantities, denoted by $\underline{\star}$. $\mathcal{R}$ is the universal gas constant. The function $\alpha = [1 + c_0(1 - \sqrt{T_r})]^2$ accounts for the polarity of a fluid and is a correlation of temperature T, critical temperature T_c and acentric factor ω via $c_0 = 0.37464 + 1.54226\omega - 0.2699\omega^2$. The parameter $a = 0.45724 \left(\mathcal{R}^2 T_c^2 / p_c \right)$ represents attractive forces between molecules and the effective molecular volume is represented by $b = 0.0778 \left(\mathcal{R} T_c / p_c \right)$.

We use conventional mixing rules to extend the PR-EOS to a mixture composed of N_c components. The parameters required in the EOS are calculated from

$$a\alpha = \sum_{i}^{N_c} \sum_{j}^{N_c} z_i z_j a_{ij} \alpha_{ij} \quad \text{and} \quad b = \sum_{i}^{N_c} z_i b_i, \tag{10}$$

with z_i being the mole fraction of component i (overall or in the liquid/vapor phase). The coefficients a_{ij} and α_{ij} are calculated with combination rules given by Harstad $et\ al.$ (1997). We calculate off-diagonal elements using the same expression as for the diagonals together with pseudo-critical parameters

$$T_{c,ij} = \sqrt{T_{c,i} T_{c,j}} (1 - \delta'_{ij}), \tag{11}$$

$$p_{c,ij} = Z_{c,ij} (\mathcal{R} T_{c,ij} / v_{c,ij}), \tag{12}$$

$$Z_{c,ij} = 0.5 \left(Z_i + Z_j \right), \tag{13}$$

$$v_{c,ij} = \frac{1}{8} \left[v_{c,i}^{1/3} + v_{c,j}^{1/3} \right]^3, \tag{14}$$

$$\omega_{ij} = 0.5 \left(\omega_i + \omega_j \right). \tag{15}$$

The binary interaction parameter δ'_{ij} is set to zero for all simulations. Caloric properties are computed with the departure function formalism based on an ideal reference state given by nine-coefficient NASA polynomials (Goos $et\ al.$, 2009) and analytical departure integrals based on the PR-EOS, see, e.g., Poling $et\ al.$ (2000) and Matheis $et\ al.$ (2016).

The single-phase frozen temperature (T_F) is computed iteratively by minimizing the objective function

$$F = \frac{\underline{e}^\star - \underline{e}_F(T_F, \underline{\rho}^\star, \mathbf{z}^\star)}{\underline{e}^\star}, \tag{16}$$

with $\underline{e}^\star = \underline{e}_{LES}$, $\underline{\rho}^\star = \underline{\rho}_{LES}$ and $\mathbf{z}^\star = \mathbf{z}_{LES}$ being the molar internal energy, molar density and overall molar composition that come from the flow solver (after conversion to molar quantities). Once the temperature is available, all other thermodynamic properties (e.g., pressure for FC formulation) and derivatives (e.g., specific heats, speed of sound, partial properties) can be calculated in a straightforward manner.

The cubic EOS yield good accuracy and computational efficiency for simulations of supercritical mixtures and single-phase liquids or gases, see, e.g., Matheis $et\ al.$ (2016). However, it is important to note that the pressure and temperature resulting from this $single\text{-}phase\ model$ may correspond to unstable thermodynamic states for mixtures that are actually located within the two-phase region.

We therefore perform vapor-liquid phase equilibrium (VLE) calculations (c.f. Qiu & Reitz, 2014) for the local fluid composition and the equilibrium pressure and temperature. During each time-step, density, internal energy and fluid composition within a finite-volume cell are passed to a thermodynamic solver in which it is tested whether this state corresponds to a point within or outside the two-phase region. A mixture is considered stable at the current temperature and pressure if and only if the total Gibbs energy is at its global minimum (Michelsen & Mollerup, 2007). Whether a split into two phases yields a decrease in the Gibbs energy, or, in other words, whether the fluid state within a computational cell lies within the two-phase region or not can be determined efficiently with the Tangent Plane Distance (TPD) function (Michelsen, 1982). If the result of the TPD test tells us that the single-phase mixture is stable, then we apply the single-phase PR-EOS in a straightforward manner. If it turns out that the mixture is unstable, which means that the fluid would prefer to exist as two phases separated by an interface, then we solve the so-called isochoric-isoenergetic flash problem (Castier, 2009). That is, temperature and pressure are iterated until the sum (weighted by the phase fraction) of the liquid-phase and vapor-phase densities and internal energies within a computational cell corresponds to the overall internal energy and partial densities that come from the flow solver. The corresponding objective function for the two-phase equilibrium model is

$$\mathbf{F} = \left\{ \frac{\underline{v}^\star - \underline{v}_{EQ}(T, p, \mathbf{z}^\star)}{\underline{v}^\star}, \frac{\underline{e}^\star - \underline{e}_{EQ}(T, p, \mathbf{z}^\star)}{\underline{e}^\star} \right\} \tag{17}$$

with $\underline{e}^\star = \underline{e}_{LES}$, $\underline{v}^\star = \underline{v}_{LES}$ and $\mathbf{z}^\star = \mathbf{z}_{LES}$ being the specific molar internal energy and volume and overall composition in the corresponding cell, respectively. In the innermost iteration loop, we solve an isothermal isobaric flash problem, i.e., we calculate the VLE at given temperature, pressure and overall composition. The necessary condition of thermodynamic equilibrium is that the fugacity f_i of each component i is the same in the liquid (subscript l) and vapor (subscript v) phase, i.e.,

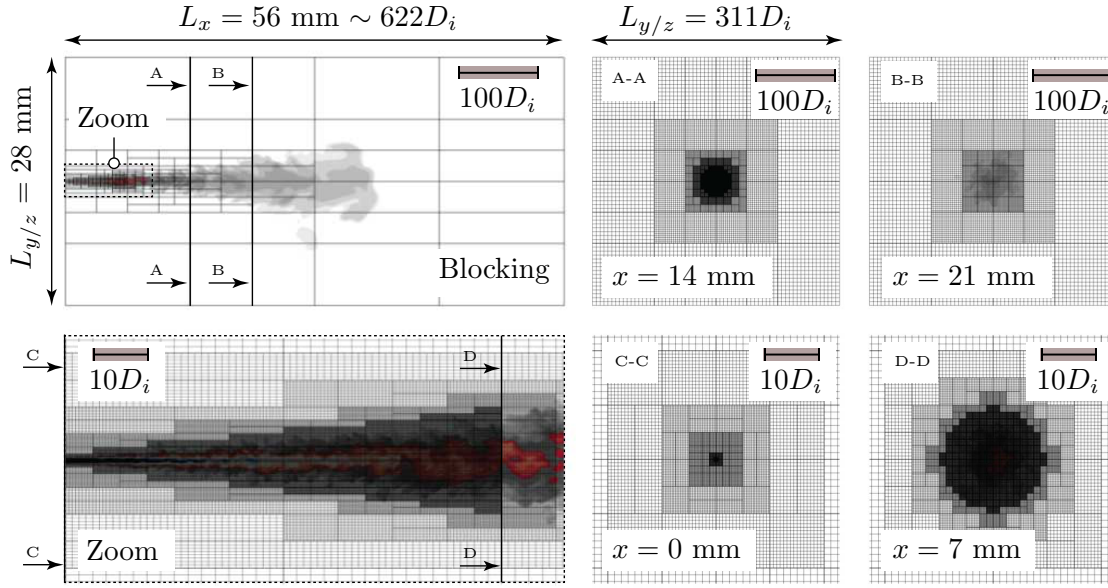$$f_{i,v}(T, p, \mathbf{y}) = f_{i,l}(T, p, \mathbf{x}). \tag{18}$$

Figure 1: Blocking and grid resolution of the computational domain. Note the different scaling of top and bottom row.

We denote liquid and vapor phase mole fractions by $\mathbf{x} = \{x_1 \dots x_{N_c}\}$ and $\mathbf{y} = \{y_1 \dots y_{N_c}\}$, respectively. The material balance for each component,

$$\psi_v y_i + (1 - \psi_v) x_i = z_i, \tag{19}$$

with ψ_v being the overall molar vapor fraction, and the requirement that mole fractions in the liquid and vapor phase must sum to unity, or equivalently

$$\sum_{i=1}^{N_c} y_i - x_i = 0, \tag{20}$$

yield $(2N_c + 1)$ equations, which are solved for the unknown compositions $\mathbf{x}$ and $\mathbf{y}$ of liquid and vapor, and the molar vapor fraction ψ_v. Equilibrium volume $\underline{v}_{EQ}$ and energy $\underline{e}_{EQ}$ are then obtained as

$$\underline{v}_{EQ}(T, p, \mathbf{z}^\star) = \psi_v \underline{v}_v + (1 - \psi_v) \underline{v}_l \tag{21}$$

$$\underline{e}_{EQ}(T, p, \mathbf{z}^\star) = \psi_v \underline{e}_v + (1 - \psi_v) \underline{e}_l. \tag{22}$$

Specific molar volumes $(\underline{v}_v(T, p, \mathbf{y}), \underline{v}_l(T, p, \mathbf{x}))$ and energies $(\underline{e}_v(T, p, \mathbf{y}), \underline{e}_l(T, p, \mathbf{x}))$ of the two phases are calculated with the EOS (Eq. 9) and the departure function formalism, respectively. Note that this model assumes that the phase-transition timescale is small compared to the flow timescale. For more details we refer to Matheis & Hickel (2016, 2017) and the literature cited therein.

NUMERICAL MODEL

The governing equations are discretized by a conservative finite-volume scheme on an adaptive Cartesian grid. Effects of unresolved subgrid scales (SGS) are modeled by the adaptive local deconvolution method (ALDM) of Hickel *et al.* (2014). The viscous fluxes are discretized using a 2nd order central difference schemes, and the 3rd order explicit Runge-Kutta scheme of Gottlieb & Shu (1998) is used for time integration.

SETUP

All simulations have been performed in a rectangular domain with the dimensions $L_x = 56$ mm ($\sim 622 D_i$) in the streamwise and $L_y = L_z = 28$ mm ($\sim 311 D_i$) in the lateral directions. D_i denotes the injector diameter. An adaptive Cartesian blocking strategy with a static local coarsening/refinement is used to allow for a varying grid resolution along the spray break-up trajectory. The grid shown in Fig. 1 consists of 2766 blocks with 7 grid refinement levels and a total number of about 15.1 million cells. At the jet inflow a time dependent mass flow rate is prescribed during the injection time of 1.5 ms. We do not prescribe any turbulent fluctuations at the inflow patch because the jet break-up process of the high-speed jet is predominantly controlled by high shear forces and very high hydrodynamic pressure fluctuations. At the outlet we prescribe the static pressure of 60 bar. All walls are modeled as adiabatic.

RESULTS

Figure 2 shows a temporal sequence of the early jet evolution (24μs-144μs). The left column shows experimental data (diffused back illumination), and the right column shows snapshots of the temperature distribution for the LES. The liquid penetration length is illustrated by the cyan iso-contour of the liquid volume fraction $LVF = 0.15\%$. We observe a very good qualitative agreement between experimental data and LES. At 24 μs the liquid n-dodecane jet extends about 6 mm into the nitrogen atmosphere; at about 44 μs the liquid length has reached its quasi-steady mean. Later points in time illustrate the vapor evolution.

The spray structure in the near-nozzle field at a very early state, 10 μs, 20 μs and 30 μs after injection start, is shown in Fig. 3. The left column are instantaneous snapshots of the temperature field (contour levels are shown for 363 K < T < 900 K, from dark to light grey shades). Superimposed is the vapor volume fraction distribution (from blue to red shades) for the two-phase region within which the isochoric-isoenergetic flash problem was solved. The right column are contours of the corresponding pressure fields (5 MPa < p < 7 MPa, from blue to red shades). We see that the dodecane-nitrogen mixture locally experiences pressures much different from the average ambient pressure. Even in the fully developed steady state we see pressure fluctuations in the shear layer in the order of magnitude of +/- 10bar. For these harsh conditions
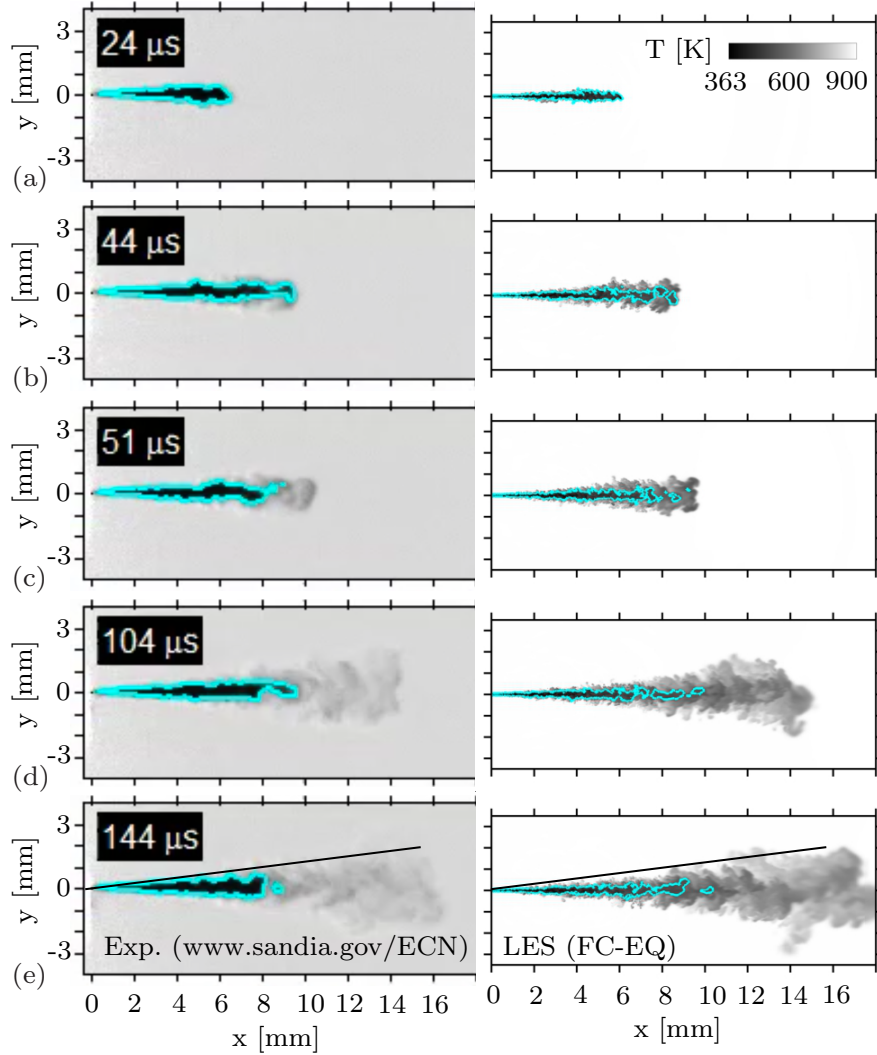
Figure 2: Temporal sequence of the injection event: left column shows experimental data of Pickett *et al.* (2011*a*); right column shows instantaneous snapshots of the temperature distribution for LES with conservative finite-volume vapor-liquid equilibrium model. Liquid penetration length is illustrated by a $LVF = 0.15\%$ iso-contour.

during the startup phase, where the jet fluid accelerates from 0 to 600 m/s in about 10 μs, LES with a single-phase dense-gas thermodynamic model usually require some kind of a stabilization method that sacrifices energy conservation in some way. Our fully conservative two-phase LES model, which allows to represent the coexistence of multicomponent subcritical two-phase states in a computational cell, surprisingly performs very well in terms of computational stability does not require any ad-hoc fixes.

One result of the VLE calculation are the vapor and liquid volume fractions (VVF and LVF), which give us a non-arbitrary quantitative definition of the jet boundary and its liquid core. Liquid droplets, which are usually detected in experiments via Mie scattering, can be expected at all locations with a VVF less then one (and much larger than zero). We define the liquid core length L_l as the rightmost location where the liquid volume fraction is $LVF = 0.01$ and the vapor penetration length L_v as the rightmost location where the dodecane mass fraction is $Y_{C12H26} = 1\%$. LES results and experimental measurements for liquid and vapor penetration trajectories are shown in Fig. 4. We observe an excellent

agreement of the vapor penetration trajectory, L_v, up to ~ 0.8ms. Slight deviations of the penetration depth at later times can be attributed to effects of numerical and experimental boundary conditions; the outflow boundary of the computational domain is indicated in the figure. We also observe an excellent agreement of L_l with the experimental time-resolved signal. It is important to note that the measured L_l depends on the chosen threshold value. Based on a thorough analysis based on Mie-scatter theory together with assumptions on droplet diameters, Pickett *et al.* (2011*a*) conclude that the LVF threshold representing their liquid length is expected to be less than 0.15% at Spray A conditions. The experimental time-averaged liquid length fluctuates by approximately ± 1mm about the quasi-steady mean of 10.4mm; this value is in excellent agreement with our LES data for the threshold value of 0.15%. In order to evaluate the sensitivity on the threshold value we computed L_l for $LVF = \{3\%, 1\%, 0.15\%, 0.05\%\}$ and obtained $L_l = \{8.83, 9.91, 10.40, 10.49\}$mm, respectively.

In the experiment, the vapor penetration length is derived from high speed schlieren images. The right panel of Fig. 4 shows an
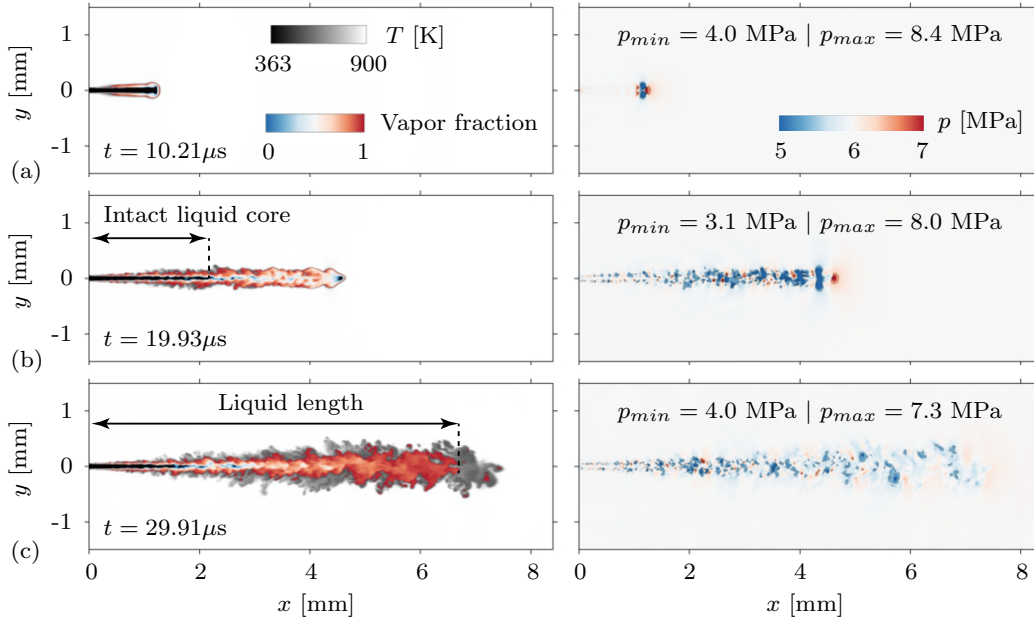
Figure 3: Left column: Instantaneous LES snapshots of the temperature field, superimposed by the vapor volume fraction distribution. Right column: Instantaneous LES snapshots of the pressure field together with the maximum and minimum pressure at the corresponding time instance.
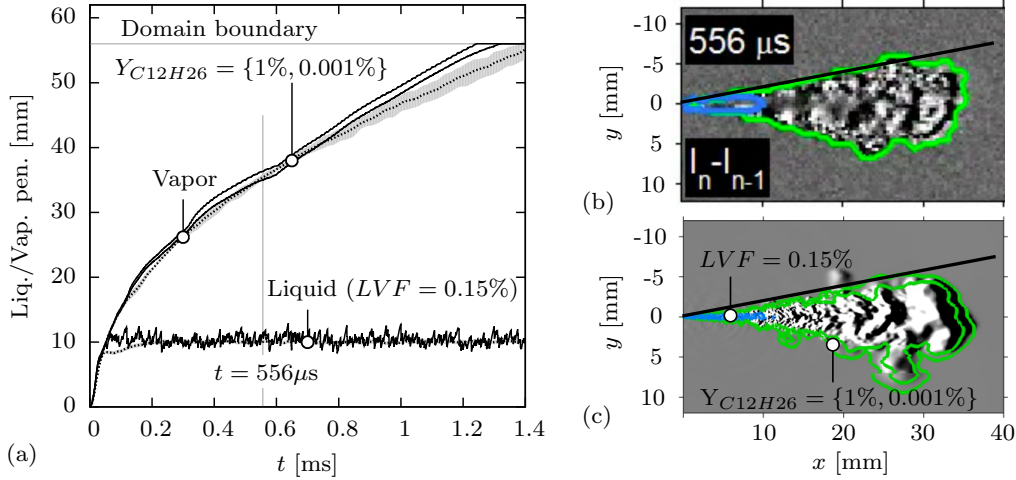

Figure 4: (a) Comparison between LES and experimental liquid and vapor penetration trajectories. (b) Experimental schlieren image. (c) Numerical schlieren image for LES. See Pickett *et al.* (2011*a,b*) for details on experimental data.

experimental and a numerical schlieren image, which are strikingly similar. The numerical schlieren image is a contour plot of the axial density gradient $\partial \rho / \partial x$ spatially averaged along the z-direction. The cyan and green lines represent the liquid core ($LVF = 0.01$) and the jet boundary ($Y_{C12H26} = 1\%$). Quantitatively, a definition of the vapor penetration depth by a 1% mixture fraction threshold seems to slightly under predict the vapor penetration derived from a schlieren image, mainly in the long term evolution. We therefore do not recommend to track values larger 1%.

CONCLUSIONS

A detailed multi-species two-phase thermodynamic equilibrium model for the Eulerian LES of turbulent mixing at high pressures has been presented and applied for LES of liquid-fuel injection at transcritical operating conditions. The thermodynamics model is based on cubic equations of state and vapor-liquid equilibrium calculations. The model accounts for fuel compressibility and effects associated with real-fluid thermodynamics, such as the solubility of ambient gas into the liquid phase or variable thermo-physical properties, and can accurately represent supercritical states as well as coexisting multi-component subcritical two-phase states. The present approach yields a thermodynamically consistent and tuning-parameter-free framework without any semi-empirical break-up and evaporation models. The only input parameters required are the NASA polynomials, the critical properties, and the acentric factor of each species, and, if available, the binary interaction parameter.

The availability of the liquid volume fraction through the homogeneous mixture approach provides a non-arbitrary definition of the liquid penetration length that can be linked to experimental measurements. Computational results for the transcritical dodecane injection ECN Spray A case demonstrate the excellent predictive per-

formance of the model. We saw that the Spray A dodecane-nitrogen mixture locally experiences pressures significantly below the nominal operating pressure of 6 MPa when the jet accelerates from 0 to 600 m/s in just 10 μs. LES with our new fully conservative multicomponent two-phase equilibrium model did not show any stability problems and yield numerical predictions that are in very good agreement with available experimental data.

Taking transcritical phase separation into account by solving the isochoric-isoenergetic flash problem on the fly improves accuracy, physical consistency and numerical stability of LES for high-pressure liquid-fuel injection. However, one should also note that this detailed thermodynamic model is computationally expensive; LES with our present VLE implementation cost about four times as much as a single-phase LES with the same real-gas EOS.

REFERENCES

Balaji, B., Raghavan, V., Ramamurthi, K. & Gogos, G. 2011 A numerical study of evaporation characteristics of spherical n-dodecane droplets in high pressure nitrogen environment. *Phys. Fluids* **23** (6), 063601.

Castier, M. 2009 Solution of the isochoric–isoenergetic flash problem by direct entropy maximization. *Fluid Phase Equilibr.* **276** (1), 7–17.

Chung, T. H., Ajlan, M., Lee, L. L. & Starling, K. E. 1988 Generalized multiparameter correlation for nonpolar and polar fluid transport properties. *Ind. Eng. Chem. Res.* **27** (4), 671–679.

Crua, C., Manin, J. & Pickett, L. M. 2015 Transition from droplet evaporation to miscible mixing at diesel engine conditions. In *ICLASS 2015, 13th Triennial International Conference on Liquid Atomization and Spray Systems, Tainan, Taiwan*.

Dahms, R. N., Manin, J., Pickett, L. M. & Oefelein, J. C. 2013 Understanding high-pressure gas-liquid interface phenomena in Diesel engines. *P. Combust. Inst.* **34** (1), 1667–1675.

Dahms, R. N. & Oefelein, J. C. 2013 On the transition between two-phase and single-phase interface dynamics in multicomponent fluids at supercritical pressures. *Phys. Fluids* **25** (9), 092103.

Goos, E., Burcat, A. & Ruscic, B. 2009 Third Millennium Ideal Gas and Condensed Phase Thermochemical Database for Combustion.

Gottlieb, S. & Shu, C. 1998 Total variation diminishing Runge-Kutta schemes. *Math. Comput.* **67** (221), 73–85.

Harstad, K., Miller, R. S. & Bellan, J. 1997 Efficient high-pressure state equations. *AIChE J.* **43** (6), 1605–1610.

Hickel, S., Egerer, C. P. & Larsson, J. 2014 Subgrid-scale modeling for implicit large eddy simulation of compressible flows and shock-turbulence interaction. *Phys. Fluids* **26** (10), 106101.

Manin, J., Bardi, M., Pickett, L. M., Dahms, R. N. & Oefelein, J. C. 2014 Microscopic investigation of the atomization and mixing processes of diesel sprays injected into high pressure and temperature environments. *Fuel* **134**, 531–543.

Matheis, J. & Hickel, S. 2016 Multi-component vapor-liquid equilibrium model for LES and application to ECN Spray A. In *Proceedings of the 2016 Summer Program, Center for Turbulence Research, Stanford University*. ArXiv preprint arXiv:1609.08533.

Matheis, J. & Hickel, S. 2017 Multi-component vapor-liquid equilibrium model for LES of high-pressure fuel injection and application to ECN Spray A. *submitted to International Journal of Multiphase Flow* .

Matheis, J., Müller, H., Lenz, C., Pfitzner, M. & Hickel, S. 2016 Volume translation methods for real-gas computational fluid dynamics simulations. *The Journal of Supercritical Fluids* **107**, 422–432.

Michelsen, M. L. 1982 The isothermal flash problem. Part I. Stability. *Fluid Phase Equilibr.* **9**, 1–19.

Michelsen, M. L. & Mollerup, J. M. 2007 *Thermodynamic Models: Fundamentals & Computational Aspects*. Tie-Line Publications.

Peng, D. Y. & Robinson, D. B. 1976 A new two-constant equation of state. *Ind. Eng. Chem. Fund.* **15**, 59–64.

Pickett, L. M., Genzale, C. L., Manin, J., Malbec, L. M. & Hermant, L. 2011*a* Measurement Uncertainty of Liquid Penetration in Evaporating Diesel Sprays. In *Proceedings of the 23rd Annual Conference on Liquid Atomization and Spray Systems*.

Pickett, L. M., Manin, J., Genzale, C. L., Siebers, D. L., Musculus, M. P. B. & Idicheria, C. A. 2011*b* Relationship Between Diesel Fuel Spray Vapor Penetration/Dispersion and Local Fuel Mixture Fraction. *SAE Int. J. Engines* **4** (1), 764–799.

Poling, B., Prausnitz, J. & O' Connell, J. 2000 *The properties of gases and liquids*. McGraw Hill Professional.

Prausnitz, J. M., Lichtenthaler, R. N. & de Azevedo, E. G. 1998 *Molecular Thermodynamics of Fluid-Phase Equilibria*. Pearson Education.

Qiu, L. & Reitz, R. D. 2014 Simulation of supercritical fuel injection with condensation. *Int. J. Heat Mass Tran.* **79**, 1070–1086.

Qiu, L. & Reitz, R. D. 2015 An investigation of thermodynamic states during high-pressure fuel injection using equilibrium thermodynamics. *Int. J. of Multiphas. Flow* **72**, 24–38.